PERGAMON

Deep-Sea Research II 50 (2003) 2389–2404

DEEP-SEA RESEARCH
PART II

www.elsevier.com/locate/dsr2

The California Current system off Monterey, California: physical and biological coupling

C.A. Collins[a,*,1], J.T. Pennington[b], C.G. Castro[a,b,2], T.A. Rago[a], F.P. Chavez[b,1]

[a] *Department of Oceanography, Naval Postgraduate School, Rm 328, 833 Dyer Road, Monterey, CA 93943-5122, USA*
[b] *Monterey Bay Aquarium Research Institute, 7700 Sandholdt Road, Moss Landing, CA 95039-0628, USA*

Received 21 October 2002; received in revised form 30 March 2003; accepted 4 April 2003

Abstract

Repeated hydrobiological surveys over the period 1988–2002 perpendicular to the central California coast indicate strong coupling between physical circulation and biological production. An equatorward-flowing jet about 100–200 km from shore marked the inshore edge of the California Current (CC). This "CC Jet" had its highest velocities during late winter and spring. The jet divided inshore, biologically productive waters from offshore, low-production waters. Mean flow in the inshore waters is poleward. However, this flow is interrupted in late spring and summer by a surface-enhanced, equatorward-flowing, coastal upwelling jet. The upwelling jet coincides with maxima of nutrients, chlorophyll-*a* and primary production. Annual variability in the inshore zone is related to (1) vertical pycnocline movements associated with geostrophic adjustments to accelerations of the California Current system, and (2) coastal upwelling. In offshore waters, the annual cycle accounted for a small fraction of the variability, indicating the dominance of eddies and meanders in this zone (J. Geophys. Res. 92 (1987) 12 947). The offshore regime was mesotrophic to oligotrophic, with a subsurface chlorophyll-*a* maximum above the nutricline. Considerable subduction may occur under the California Current jet and be an important process in the export of biogenic material to the deep sea.
Published by Elsevier Ltd.

1. Introduction

The California Current (CC) is the eastern limb of the North Pacific subtropical gyre and flows from Oregon to Baja California. At its mid-point off central California the CC transports subarctic surface waters (0–500 m) southwards about 150–1300 km from shore (Lynn and Simpson, 1987, Collins et al., 2000). Seasonal northwesterly winds, that are in part responsible for the CC, generate coastal upwelling. Inshore of the CC equatorial waters are transported poleward by the California Undercurrent (CUC) and the surface (Davidson) Inshore Current (IC). The IC also transports Subarctic waters that have been recirculated either in the Southern California bight or elsewhere. The mean circulation is strongly modified by energetic subseasonal and mesoscale circulation (Lynn and Simpson, 1987). The region between the CC and

*Corresponding author. 1400 Fredericks, San Luis Obispo, CA 93405, USA. Tel.: +1-813-656-3271; fax: +1-813-656-3686.
E-mail address: collins@nps.navy.mil (C.A. Collins).
[1] These authors contributed equally to this research.
[2] Current address: IIS CSIC, Eduardo Cabello, 6, 36208, Vigo, España.

0967-0645/$ - see front matter Published by Elsevier Ltd.
doi:10.1016/S0967-0645(03)00134-6

the CUC is called the Coastal Transition Zone and is marked by meanders and mesoscale eddies (Brink and Cowles, 1991). This combination of currents, eddies and upwelling circulation is referred to as the California Current system (CCS).

Earlier studies depended upon data obtained by the California Cooperative Fisheries Investigations (CalCOFI), which consisted of low resolution hydrography and vertical profiles to only 500 m (Lynn et al., 1982, Chelton, 1984, Lynn and Simpson, 1987). Seasonal variability was reviewed by Hickey (1998). She concluded that the CC and CU have seasonal maxima in summer to early fall while the IC is strongest in winter. Changes in water properties deeper than about 75 m were reported to be due to vertical movement of density surfaces in response to winds and currents, and to a lesser extent to horizontal advection of water properties along density surfaces (Lynn and Simpson, 1987). Above 40 m, maximum density was observed during February–March. Studies of seasonal variability in Monterey Bay include Skogsberg (1936), Skogsberg and Phelps (1946), Abbott and Albee (1967), Kuo (1991), and Pennington and Chavez (2000). These studies document a shoaling of the thermocline and halocline in Monterey Bay from February through June. In Monterey Bay, surface waters were coldest and saltiest in spring, warmed during summer, freshened in the fall, and cooled and freshened further in winter.

The primary physical, chemical and biological data for this paper come from a high-resolution hydrographic section oriented perpendicular to the coast at Moss Landing, California, along CalCOFI Line 67 (Fig. 1). This section was logistically convenient for research vessels based in Moss Landing and took advantage of continuing observational efforts in Monterey Bay by the Monterey Bay Aquarium Research Institute (MBARI) and the Naval Postgraduate School (NPS). The focus of this paper is on the seasonal circulation and its relationship to coastal upwelling and biological production. Data collection and processing procedures are discussed, and then time series of physical, chemical and primary productivity are presented and seasonal patterns determined.

2. Data and methods

The basis for this paper is hydrographic data collected by NPS and MBARI beginning in April 1988 along CalCOFI Line 67. During the period from April 1988 to April 1991, sampling occurred from station 80 (35°47.2′N, 124°11.7′W) into Monterey Bay where the position of inshore stations varied (Rago et al., 1997). Note that there was a 3-month delay to the second cruise in July 1989 and that during the first year there were few observations farther than 170 km from shore. Beginning in September 1988, these bimonthly cruises were supplemented with biweekly cruises in Monterey Bay (Rosenfeld et al., 1994a, Pennington and Chavez, 2000). Cruises along Line 67 resumed in February 1997 with hydrographic stations spaced at 10 n. mile (18.5 km) intervals (see Fig. 1) to resolve the distribution of mass at the local internal Rossby radius of deformation (Rosenfeld et al., 1994b). CTD stations extended to 1000 dbar where water depth permitted. Note that the trend of the California coastline outside Monterey Bay intersects Line 67 about 30 km from shore.

Beginning in 1997, 80 h were allocated for each cruise along Line 67, and in all but extreme weather conditions sampling occurred offshore to station 90 (35°27.2′N, 124°54.2′W), a distance of 315 km from the coast. Station 90 is located near the mean position of the axis of the CC as defined by the salinity minimum on $\sigma_t = 25$ (Lynn and Simpson, 1987, Fig. 8). The station closest to shore was located within Monterey Bay at the head of Monterey submarine canyon where the water is 240 m deep. The elapsed time between the first and last station was usually 60 h.

Methods used to collect hydrographic data were given by Rago et al. (1997) for 1988–1991 and Asanuma et al. (1999) for subsequent cruises. A NBIS™ Mk IIIb CTD was used for the earlier effort and a SeaBird™ 911 for the latter period. CTD data were processed using software provided by the manufacturers for their respective instruments, and data were averaged into 2-dbar bins. Derived quantities (density anomaly and geopotential anomaly) were computed using the 1980 Equation of State. Methods for biological and

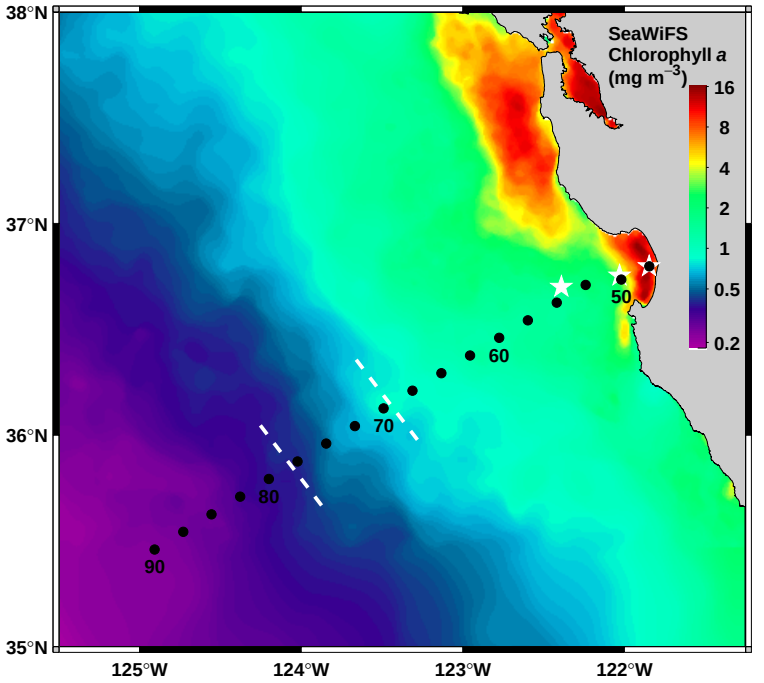

Fig. 1. Station locations along Line 67 are shown with black dots and triweekly survey stations are indicated with white stars. Every fifth station is labeled. The background is the April–June mean chlorophyll field for 1999–2002 estimated by SeaWiFS. The white dashed lines mark the mean April–June position of the California Current jet (see text). It marks the transition from the high productive ($>1\,\mathrm{mg\,m^3}$) coastal and the low chlorophyll ($<0.2\,\mathrm{mg\,m^3}$) offshore oligotrophic waters.

chemical measurements (these did not begin until 1989) have been described by Chavez et al. (2002) and Pennington and Chavez (2000).

For coastal waters, Eulerian and Lagrangian time scales are 5 and 10 days, respectively (Collins et al., 1996; Garfield et al., 1999). This means that each of our sections can be considered both synoptic and independent. It also means that the ~2-month sampling interval does not provide good temporal resolution for the evolution of the synoptic scale fields.

Data are shown as a function of time and distance from shore. Statistics were computed by binning the data as a function of distance from shore. To accommodate the varying density of observations, different bin sizes were used: 5 km from 0 to 10 km, 10 km from 10 to 200 km, and 20 km from 200 to 320 km. Data from adjacent bins were combined and used for curve fitting and statistics. As a result, adjacent statistical estimates are not independent.

Seasonal variability can be examined by either averaging data by month or season or by fitting a harmonic to the data. Chelton (1984, Appendix A) discussed these approaches, and harmonic fitting was used in this study due to irregular spatial and temporal sampling. Procedures for least-squares harmonic fitting followed Lynn (1967) and used MATLAB™ routines developed by Steger (1997). The harmonic function used the general form $Y(t) = A_0 + \Sigma A_i \cos(2\pi\omega_i t - \phi_i)$, where A_0 is the residual, t the time in years, and the summation includes n discrete frequencies ω_i (cycles per year), amplitudes A_i, and phases ϕ_i. Note that phase represents the time at which the oscillation, $Y(t)$, is maximum. Models that included both annual and semiannual frequencies as well as a model that contained only the annual frequency were fit to combined bins and plotted (Lynn, 1967, Fig. 13). Results resemble those shown by Lynn (1967) for stations 70–52 and 70–70. Inclusion of the semiannual harmonic did not significantly improve

the percent of the variance accounted for by the fit, and increased the variability of amplitude and phases for those cases where the model accounted for only a small percent of the variability. As a consequence, only the results for model with the annual harmonic were used.

The 1997–1998 El Niño resulted in a strong non-seasonal perturbation to the hydrographic data, and least-squares fitting of the annual cycle was significantly improved by not including the El Niño data (July 1997–June 1998). Statistics and an annual cycle were calculated from these "no El Niño" data as a function of distance from shore along Line 67 and include means, standard deviations, and the fit of a sinusoid with annual frequency.

3. Results

3.1. Dynamic height

Dynamic thickness was calculated for three layers, an upper layer (0–200 dbar), an intermediate layer (200–500 dbar), and a deep layer (500–1000 dbar). The mean dynamic height and its standard deviation as a function of distance from shore are shown in Figs. 2a and b. The dynamic height for the upper layer was lowest within Monterey Bay, less than 0.4 dynamic meters. Immediately outside the Bay, the dynamic height increased to about 0.41 dynamic meters (implying southward geostrophic flow across the entrance to the Bay) and it remained nearly level between 30 and 80 km from shore. Between 80 and 250 km from shore, the dynamic thickness increased at a nearly constant rate, 0.01 dynamic meters per 20 km. This region marked the strong southward flow along the inshore portion of the CC.

The mean profile for the intermediate and deep layers had a different shape than the upper layer (Fig. 2a). The intermediate (deep) layer had a trough at 130 (185) km from shore with maximum dynamic thickness at the coast (35 km from shore). The difference between the maximum and minimum mean dynamic height was 0.026 (0.020) dynamic meters. The mean profiles for the lower layers indicate that the choice of a reference layer

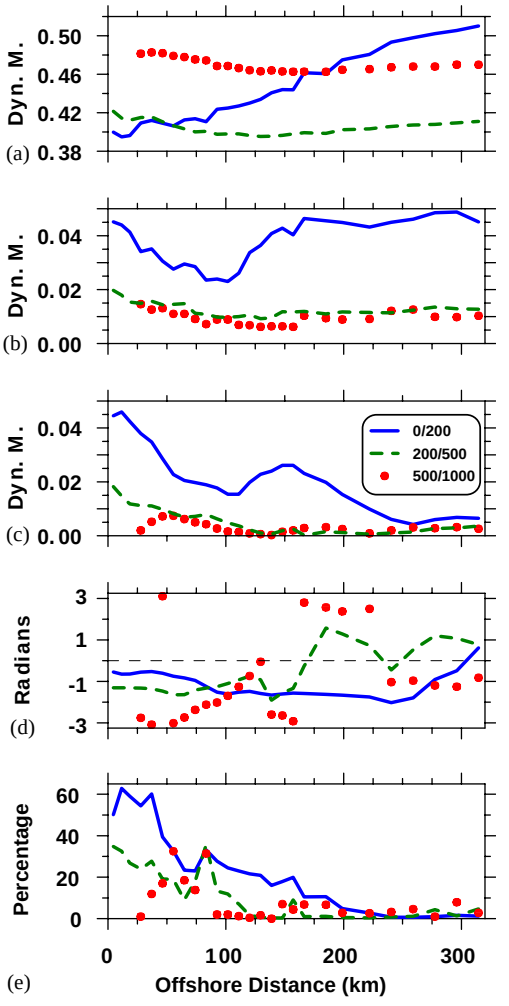

Fig. 2. Offshore profiles of dynamic height along Line 67. (a) Mean. (b) Standard deviation. (c) Amplitude of annual cycle. (d) Phase of annual cycle. Phase represents the time at which the cycle is maximum; a value of $\pi/2$ ($-\pi/2$) corresponds to April 1 (October 1). (e) Percent of variance accounted for by the annual cycle.

is crucial for determining the direction of the alongshore geostrophic flow at the sea surface. A deep reference layer will create a dynamic ridge (maximum in dynamic height) near the coast and a trough (minimum in dynamic height) at a distance of 100 km from the coast.

The offshore profiles of the standard deviation of dynamic height are shown in Fig. 2b. Lynn and Simpson (1987, Fig. 4d) show the standard

deviation of dynamic height to be largest offshore and smallest at the coast. In contrast, results shown in Fig. 2b had a well-defined maximum at the coast for all layers, probably due to the higher horizontal resolution of these data near the coast. The standard deviation for the upper layer was more than twice that of the other layers within 100 km of the coast but farther offshore, was 4 times as large. Minimum standard deviation was less than half the maximum and occurred at 100, 130, and 150 km from shore for the upper, intermediate and deep layers, respectively. Largest standard deviation was observed at the coast for the lower two layers. The maximum for the upper layer was slightly greater offshore than at the coast. From 170 km to the offshore edge of the data, the standard deviation of the upper (middle) layer was almost constant, about 0.045 (0.011) dynamic meters.

Fig. 3 shows the temporal evolution of the dynamic thickness of these three layers. El Niño was marked by a thickening of all three layers during July 97–July 98 and appeared to migrate offshore with time (Collins et al., 2002). The tightest gradients of dynamic height for the upper layer occurred between 0.45 and 0.49 dynamic meters (Fig. 3, upper). This 0.45–0.49 dynamic meter region marked strong equatorward near surface flow that usually occurred on the inshore edge of the CC. This feature will subsequently be referred to as the "CC jet."

The intermediate layer (Fig. 3, middle) had a broad trough outlined by the 0.4 dynamic meter isostere. This trough was centered about 100–150 km from shore during 1988–1991 and 2000–2002. This trough marked the transition between the coastal poleward flow of the CU and the offshore, equatorward flow of the CC. The variability of the dynamic thickness of the 200–500 and 500–1000 dbar layers (Fig. 3, lower) was similar. Note that CalCOFI sampled to 1000 dbar initially but that this was discontinued because the lower 500 dbar were not very interesting (J.L. Reid, personal communication). The correlation

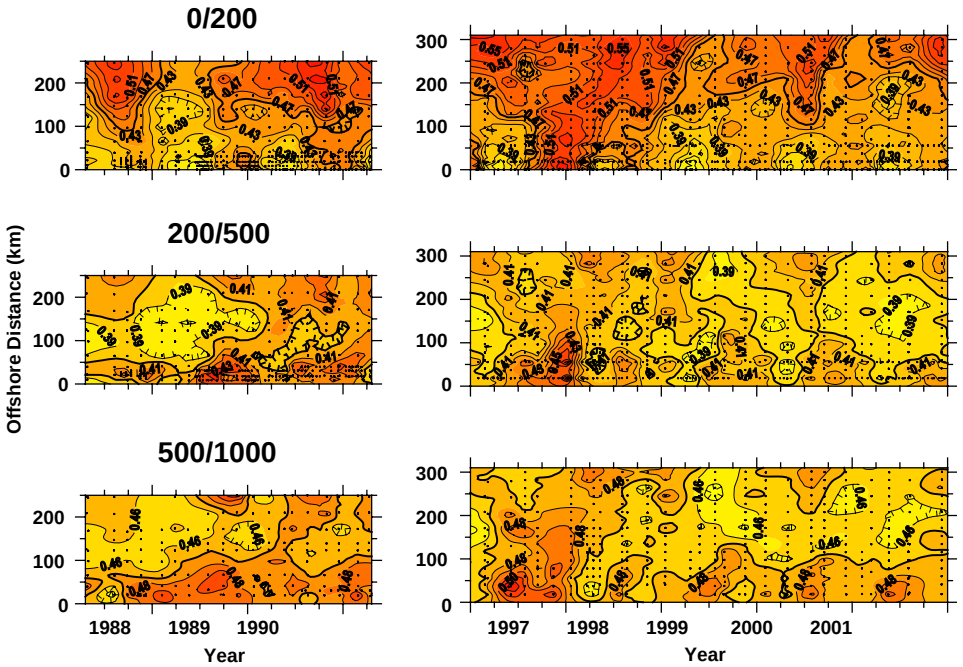

Fig. 3. Evolution of dynamic height along Line 67 with time. (upper) 0/200 dbar. The contour interval is 0.02 dynamic meters and the bold isostere is 0.45 dynamic meters (middle) 200/500 dbar. The contour interval is 0.01 dynamic meter and the bold isostere is 0.40 dynamic meters (lower) 500/1000 dbar. The contour interval is 0.01 dynamic meter and the bold isostere is 0.47 dynamic meters.

between the thickness of the deepest layer with the 200–500 dbar layer was 0.72 and the linear regression relationship was $\Delta D_{500/1000} = 0.22 + 0.62\Delta D_{200/500}$ with a standard error of 0.01 dynamic meters.

The deepest layer (Fig. 3, lower) also was characterized by a broad trough, outlined by the 0.47 dynamic meter isostere, which was centered about 150–200 km from shore. A coastal maximum occurred in late June or July from 1997 to 2001 and was greatest preceding the 1997–1998 El Niño. During 1988–1991, the summer coastal maximum was observed only in 1989.

3.2. Density surfaces

Contours of the pressure of three isopycnal surfaces, $\gamma_\theta = 25.8$, 26.2, and 26.8 kg/m^3, are shown in Fig. 4. At fixed latitude, geostrophic flow is directed along isobars at a rate proportional to their gradient. Poleward flow occurs when the pressure of the isopycnal increases toward the coast, and equatorward flow occurs where pressure decreases towards the coast (assuming a level of no motion deeper than the isopycnal). The low-density surface was chosen to be as shallow as possible without intersecting the sea surface. (The Line 67 sections had a maximum sea-surface density anomaly of 25.76 kg/m^3). The middle density surface passed through the velocity maximum associated with the California Undercurrent. The deep density surface is where the contrast between the intermediate waters from the North Pacific and Equatorial regions was greatest.

In normal years, the 25.8 kg/m^3 (26.2 kg/m^3) isopycnal upwelled to less than 40 (80) dbar between March and July at the coast (Fig. 4, upper and middle). The 26.8 kg/m^3 isopycnal was shallowest at the coast during March to April (Fig. 4, lower). In some years the 25.8 kg/m^3 isopycnal behaved like a teeter–totter, upwelling at the coast while it deepened offshore (Fig. 4, upper). This occurred in 1988, 1990, 1997, 1998, and 2000. However, in 1989, 1999, and 2001, upwelling occurred at nearly the same time along the entire section. The 26.2 kg/m^3 isopycnal behaved in a similar manner (Fig. 4, middle). The deepest isopycnal, 26.8 kg/m^3, had nearshore maxima

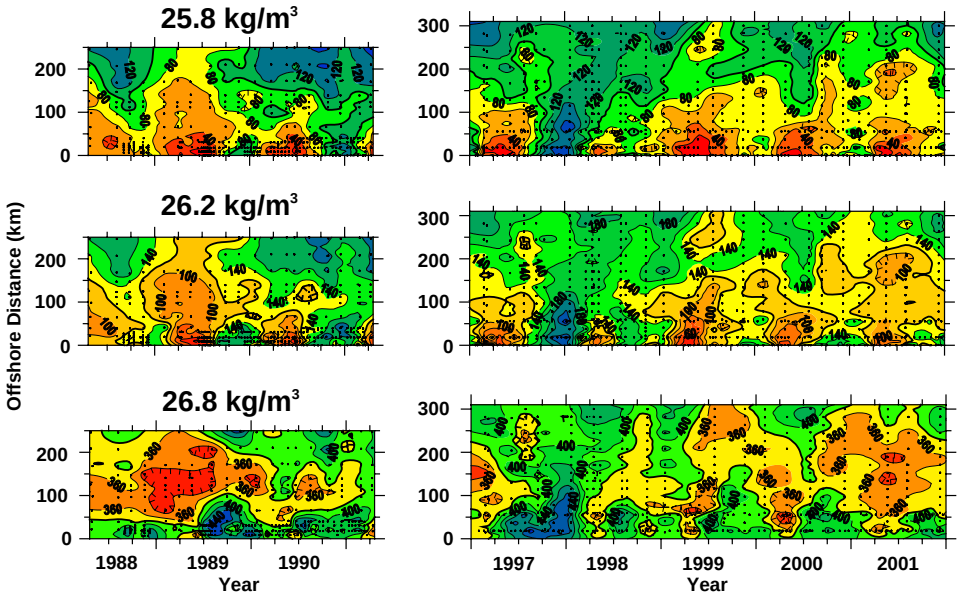

Fig. 4. Evolution of the pressure of isopycnals ($\gamma_\theta = 25.8$, 26.2 and 26.8 kg/m^3) along Line 67 with time. Contour interval is 20 dbar. (upper) 25.8 kg/m^3. The bold isobar is 100 dbar (middle) 26.2 kg/m^3. The bold isobar is 120 dbar (lower) 26.8 kg/m^3. The bold isobar is 380 dbar.

exceeding 400 dbar that occurred between 30 and 50 km from July through October (Fig. 4, lower). A pressure minimum was always observed on the 26.8 kg/m^3 isopycnal, usually between 50 and 200 km from shore. The 1997-98 El Niño was marked by an 80–100 dbar pressure increase in late fall 1997 for all three isopycnals, which appeared to move offshore with time (Fig. 4, see also Collins et al., 2002). Nearshore upwelling seasons centered on April 1999, 2000, and 2001 appeared to propagate offshore at the same speed as the deepening associated with the El Niño in late 1997.

3.3. Water mass characteristics

Temperature and salinity contrasts were large near the surface due to differences between the low temperature, high salinity of upwelled coastal waters, and the warmer temperature, low salinity of Subarctic surface waters carried southward by the CC jet (Fig. 5, upper and middle). The offshore salinity minimum in the CC often occurred subsurface at pressures as great as 70 dbar, so the vertically averaged properties for the upper 80 dbar layer were used to describe the variability of temperature and salinity. Surface-layer temperature and salinity variability were dominated inshore by seasonal changes. Temperature minima occurred in the surface layer at the coast during April or May (Fig. 5, upper) and were followed, about a month later, by a salinity maximum at the coast (Fig. 5, middle). Offshore, temperature maxima were observed from summer through fall, but the determination of the exact month of these events for a given year was difficult to determine due to poor temporal resolution of the data. In addition to seasonal features, El Niño was prominent, characterized by a late fall temperature maximum at the coast, which was followed in winter 1998 by nearshore freshening from the surface to intermediate waters.

During most periods, 33.3 or 33.4 marked a region of strong horizontal salinity gradients, marking the transition between saltier waters upwelled at the coast and the fresher offshore waters (Fig. 5, middle). These isohalines, marking

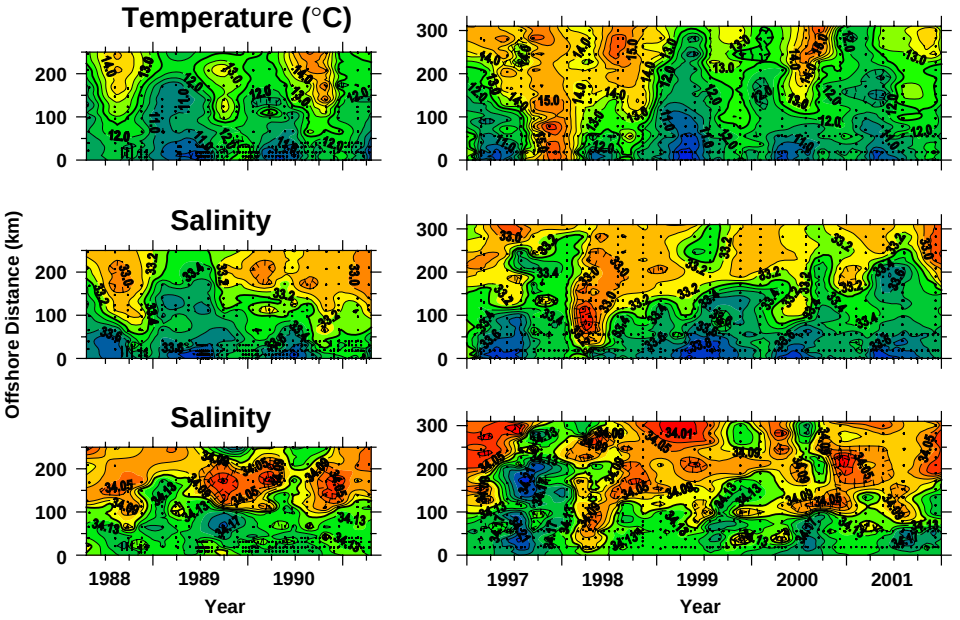

Fig. 5. (upper) Evolution of the pressure-averaged temperature for the upper 80 dbar along Line 67 with time. The contour interval is 0.5°C and the bold isotherm is 12.5°C (middle). Evolution of the pressure-averaged salinity for the upper 80 dbar along Line 67 with time. The contour interval is 0.1 and the bold isohaline is 33.3 (lower). Salinity on the isopycnal $\gamma_\theta = 26.8$ kg/m^3. Contour interval is 0.02 and the bold isohaline is 34.11.

the salinity front in the upper layer, did not have a strong seasonal pattern but appeared to vary with a longer time scale. For example, the front moved toward the shore in 1989–1990 and offshore from 1998 to 2001.

For the intermediate level at 26.8 kg/m^3, the salinity ranged from 34.01 to 34.21 (Fig. 5, lower). The midpoint of this range, the 34.11 isohaline, was used to mark the boundary between the offshore subarctic and inshore equatorial waters. The strongest temporal changes on the 26.8 kg/m^3 surface were associated with the 1997–1998 El Niño, which was marked by an increase in salinity to 34.21 in July 1997 within 100 km of shore. This preceded the warming and offshore penetration of upper layer salt by three months. Subsequently, in March and April 1998, freshening to 34.08 was observed on the 26.8 kg/m^3 isopycnal, at the same time as the upper 80 dbar freshened to 32.8 between 50 and 100 km from shore. Collins et al. (2002) attribute this freshening to onshore movement of CC and North Pacific Intermediate waters.

3.4. Nutrients, chlorophyll-a, and primary productivity

Nitrate, chlorophyll-*a*, and primary production were integrated over the euphotic zone (or 80 dbars in the case of nitrate) and contoured (Fig. 6). Inshore, clear seasonal cycles in nitrate, chlorophyll-*a* and primary production are in phase with each other and upper layer salinity but out of phase with upper-layer temperature. Highest levels were found during the summer and lowest levels during the winter. Nitrate values lower than 2 μmol/kg were observed during El Niño from November 1997 to January 1998 (Fig. 6, upper). This was in sharp contrast to the subsequent period, when nutrient-rich upwelled waters reached as far as 300 km offshore. Nitrate levels greater than 4 μmol/kg were not observed offshore of the CC jet (hatched areas of Fig. 6). Phosphate and silicate horizontal distributions were very similar to nitrate horizontal distributions (not shown). Significant positive correlations of these nutrients with nitrate were observed ($r > 0.91$) in all cases.

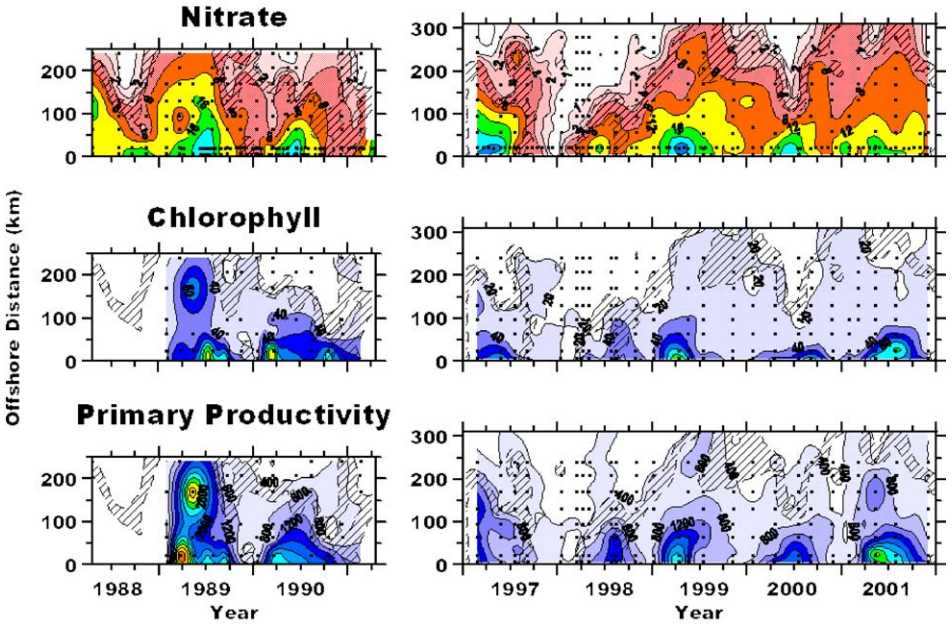

Fig. 6. Evolution of chemical and biological properties along Line 67 with time. Hatched region corresponds to dynamic heights between 0.45 and 0.49 dynamic meters. (upper) Nitrate averaged over the upper 80 dbar, 1, 2, and 4 μmol/kg values are contoured and for values greater than 4 μmol/kg the contour interval is 4 μmol/kg. (middle) Chlorophyll-*a* averaged over the euphotic zone, contour interval is 20 mg/m^2. (lower) Primary productivity averaged over the euphotic zone, contour interval is 400 mg C/(m^2 d).

Table 1
Seasonal means and standard errors of the mean of the pressure of the chlorophyll-*a* maximum by domain (Coastal, California Current Jet, and Offshore)

	Chlorophyll-*a* maximum pressure		
	Coastal	Jet	Offshore
FMA	12±12	17±16	55±29
MJJ	12±13	24±12	59±18
ASO	12±11	39±19	52±13
NDJ	11±14	19±16	38±22

Values are in decibars.

The time evolution of chlorophyll-*a* along Line 67 resembled nitrate (Fig. 6, middle). The CC jet bounded the oceanward extension of 20 mg/m^2 of integrated chlorophyll-*a* in the euphotic zone. A similar pattern was observed at the sea surface using SeaWiFS chlorophyll-*a* (Fig. 1). Maximum chlorophyll-*a* values inshore of the jet were registered close to sea surface, while offshore, there was a subsurface maximum. Table 1 shows the seasonal averages of the depth of the subsurface chlorophyll-*a* maximum. In the nutrient rich upwelled waters, the chlorophyll-*a* maximum was located on average at 12 dbar with no significant seasonal variation. In contrast in the offshore region the chlorophyll-*a* maximum depth varied between an average of 38 dbar in the winter (November–January) to 59 dbar during summer (May–July).

The temporal pattern for primary production integrated over the euphotic zone (Fig. 6, lower) was similar to that for chlorophyll-*a* and nitrate with largest values found inshore in spring and summer each year. The CC jet delimited the coastal domain of high productivity (>600 mg C/(m^2 d)) as it did for nitrate and chlorophyll-*a*. There was some decoupling between nutrient levels, phytoplankton biomass (chlorophyll-*a*) and primary production at the outer margins of the coastal upwelling domain.

3.5. Annual cycles

Offshore profiles of amplitude, phase, and the percent of the variance of dynamic height explained by the annual harmonic are shown in Figs. 2c and e. The amplitude for the upper (intermediate) layer was largest closest to shore, about 0.05 (0.02) dynamic meters and explained about 50% (35%) of the variance. These amplitudes agree with those presented by Lynn and Simpson (1987, Figs. 2b) although the data in Fig. 7c do not go far enough from the coast to observe the >0.45 dynamic meters offshore maximum at longitudes greater than 126°W at 35°N. The deep layer had largest amplitude at a distance of 55 km from shore, 0.01 dynamic meters, and explained 30% of the variance. The amplitudes decrease offshore where the annual cycle explained almost no variance at offshore distances of 250, 120 and 90 km for the upper, intermediate and deep layers.

The annual cycles for dynamic height as well as those for other physical and biological parameters are shown in Fig. 7. The dynamic heights of the upper 200 dbar layer were characterized by a nearshore minimum (maximum) in May (November) and a trough (minimum) between October and January at about 60 km from shore (Fig. 7a). The poleward flow inshore of this trough is usually called the IC. The region of strong gradient offshore, near 0.47 dynamic meters, corresponded to the CC jet, and oscillated from 210 km in March to 150 km in September.

The coastal maximum and minimum in the intermediate 200/500 dbar layer (Fig. 7b) occurred about a month earlier than for the upper layer. The intermediate layer had a well-defined offshore trough for the entire year. This trough was marked by the 0.40 dynamic meter isostere which was 100 km (150 km) from shore in May (November). Seasonal variability in this layer was weak offshore.

Year round, the deep (500/1000) dbar layer had a well-defined coastal maximum which migrated slightly offshore and was thickest during June to July (Fig. 6c). Like the layer above, a trough existed year round in the 500/1000 dbar layer, here marked by the 0.465 dynamic meter isostere and centered slightly farther from shore, about 150 km. The inshore gradient between these features was strongest near the 0.475 dynamic meter isostere and this nearshore region of strong offshore directed pressure gradient is a region of poleward flow identified with the California Undercurrent.

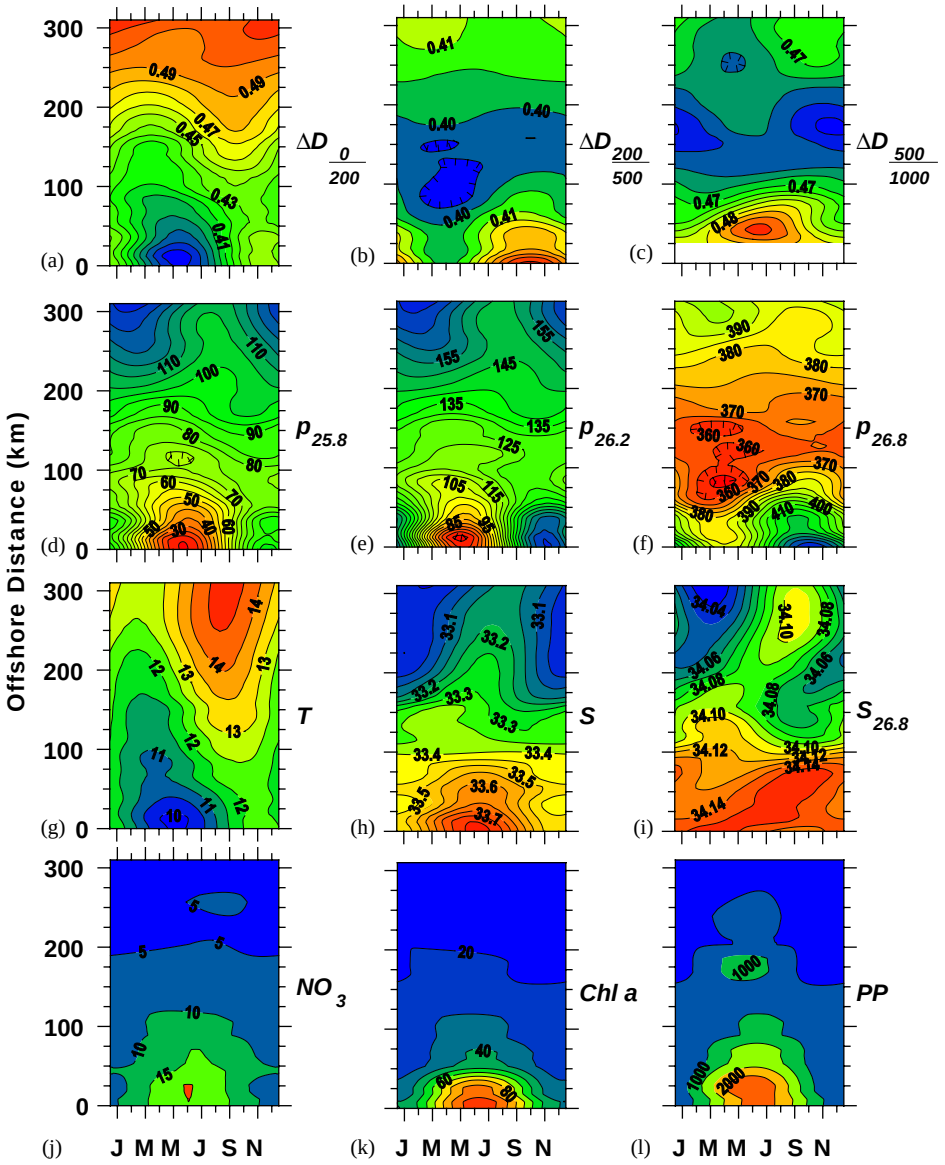

Fig. 7. Annual cycle along Line 67. Letters beneath the abscissa correspond to months and are placed beneath tick marks that correspond to the first day of the month. (a) Dynamic thickness 0/200 dbar, contour interval is 0.01 dynamic meters. (b) Dynamic thickness 200/500 dbar, contour interval is 0.005 dynamic meters. (c) Dynamic thickness 500/1000 dbar, contour interval is 0.0025 dynamic meters. (d) Pressure of the $\gamma_\theta = 25.8\,\mathrm{kg/m^3}$ isopycnal, contour interval is 5 dbar. (e) Pressure of the $\gamma_\theta = 26.2\,\mathrm{kg/m^3}$ isopycnal, contour interval is 5 dbar. (f) Pressure of the $\gamma_\theta = 26.8\,\mathrm{kg/m^3}$ isopycnal, contour interval is 5 dbar. (g) Vertically averaged temperature for the upper 80 dbar, contour interval is 0.5°C. (h) Vertically averaged salinity for the upper 80 dbar, contour interval is $S = 0.05$. (i) Salinity on the $\gamma_\theta = 26.8\,\mathrm{kg/m^3}$ isopycnal, contour interval is $S = 0.01$. (j) Vertically averaged nitrate for the upper 80 dbar, contour interval is 5 μmol/kg. (k) Chlorophyll-*a* averaged over the euphotic zone, contour interval is $10\,\mathrm{mg/m^2}$. (l) Primary productivity averaged over the euphotic zone, contour interval is $500\,\mathrm{mg\,C/(m^2 d)}$.

Consistent with the phase relationships shown in Fig 2e, the June–July coastal maximum in dynamic height in the deep layer appeared to move upward with time, appearing at the surface only in November.

The annual variability of the pressure on the 25.8 and 26.2 kg/m^3 isopycnals were similar (Figs. 7d and e), with the 25.8 kg/m^3 isopycnal upwelled at the coast from March through August and during the rest of the year downwelled toward the coast from a distance of 50–90 km from shore. The 26.2 kg/m^3 isopycnal led the 25.8 kg/m^3 at the coast by several weeks. The annual pattern for the 26.8 kg/m^3 isopycnal was quite different (Fig. 7f), downwelling toward the coast from a distance of 75–120 km year round. At the coast, the 25.8 kg/m^3 isopycnal was shallowest in May and deepest in November. Offshore profiles for the pressure of the isopyncals are not shown, but near the coast, the annual cycle of isopycnal depth accounted for more than 50% of the variability of the two shallow isopycnals but only about 20% of the variability of the 26.8 kg/m^3 isopycnal. This decreased to less than 10% for all three density surfaces at 100 km or more from shore.

The annual cycles of temperature and salinity of the upper (0–80 dbar) layer and the salinity on the deep 26.8 kg/m^3 isopycnal are shown in Figs. 7g–i. In the upper layer, typical maritime conditions occurred offshore with minimum temperature (salinity) of about 13°C (33.05) in March (February) and maximum temperature of about 14.5°C (33.15) in September (August). At the coast, surface conditions were related to coastal upwelling with minimum temperature (10°C) in May followed by maximum salinity (33.8) in June. At about 100 km from shore, little or no variation in salinity occurred either at the surface or the 26.8 kg/m^3 isopycnal layer. On the 26.8 kg/m^3 isopycnal, maximum salinity occurred in September both at 50–75 km from the coast as well as from 250 to 300 km from the coast and the lowest salinity occurred 6 months earlier. The upper layer results are similar to those reported by Lynn (1967) for 10 m depth, although his offshore salinity minimum occurred in May. In Monterey Bay, the annual cycle of temperature and salinity was similar to that reported by Pennington and Chavez (2000). The annual cycle for the upper-layer temperature (salinity on the 26.8 kg/m^3 isopycnal) included 60% (9%) of the variance at the coast which decreased (increased) to 30% (30%) at 315 km from shore. The annual cycle for the upper-layer salinity also accounted for 60% of the variance at the coast but this decreased to near zero in the region between 90 and 150 km from shore and then increased gradually to 30% at 315 km from shore.

The annual cycles obtained by harmonic fitting of nitrate, chlorophyll-*a* and primary production (Figs. 7j–l) show strong seasonal cycles nearshore. Maximum values occurred in June or July, with nitrate leading chlorophyll-*a* and primary production by several weeks. Farther than about 100 km from shore, annual variability was much reduced except for primary production (Fig. 7l), which had a second maximum at about 175 km from shore in May and June as noted above. The seasonal models accounted for about 30–40% of the variance at the coast (data not shown), but offshore the annual cycle typically accounted for 10% or less of the variance of these variables.

4. Discussion

The CC jet (represented by the isosteres of 0.45–0.49 dynamic meters for the upper 200 dbar layer) effectively divide the distributions of nitrate, chlorophyll-*a*, and primary production into coastal and offshore domains (Figs. 1 and 6). Inshore of the CC jet, nitrate exceeded 5 μmol/kg, integrated chlorophyll-*a* exceeded 20 mg m^{-2}, and integrated primary productivity exceeded 800 mg C m^{-2} d^{-1}. The offshore region was marked by the warmest and freshest waters (except during El Niño) in the upper layers and dynamic height gradients that were weaker than those found in the CC jet. Although the variability of dynamic height in the offshore region was almost the same as at the coast, the annual cycle captured less than 10% of its variance, implying that eddies and meanders dominate this region (Lynn and Simpson, 1987). In contrast, the inshore domain was dominated by the annual variability associated with coastal upwelling.

4.1. Geostrophic velocities

To examine current patterns, geostrophic velocities were computed for the surface and 200 dbar using a 1000 dbar reference level (Fig. 8). For the inner 30 km, where the data extended to only 500 dbar, the dynamic heights of the 500/1000 dbar layer next to the coast were used. The offshore profiles of dynamic height were smoothed with a 5-weight Hanning filter. This did a good job of fitting the slopes of dynamic height associated with the CC and the IC and CUC, but reduced the amplitude of a ridge in dynamic height that occurred off Monterey Bay from April through July.

The zero isotach at 200 dbar, which was located about 150 km from shore (Fig. 8b), marked the division between poleward flowing coastal waters as well as the inshore edge of the overlying CC jet. At the surface the inshore edge of the CC jet was marked by the −6 cm/s isotach closest to shore (Fig. 8a). The CC jet was strongest in March and April when equatorward flow between 150 and 200 km from shore exceeded 10 cm/s. The CC jet was weakest in the September–October period when the strongest flow slowed to about 6 cm/s. At 200 dbar (Fig. 8b), the core of equatorward flow was about 50 km further offshore, flowing only about 2 cm/s.

The pattern of flow in the inshore region was more complex. The poleward flowing surface currents next to the coast were interrupted in summer by a shallow equatorward flow across the entrance of Monterey Bay. Rosenfeld et al. (1994b) identify this feature as an upwelling jet that originated to the north in the upwelling zone off Año Nuevo, California (37°10′N). This seasonal upwelling jet is distinct from and well inshore of the CC jet discussed above. During the fall and winter when the upwelling jet was not present, there appeared to be two distinct two cores of the IC (poleward flow), one about 50 km from the coast and the other at the coast. Both were strongest in November and December when they exceeded 10 cm/s. Beginning in February, the IC weakened and was split by the upwelling jet that was centered about 25 km from the coast. The upwelling jet strengthened through May when it exceeded 8 cm/s and extended to the coast. As the upwelling jet subsequently weakened, the IC first reappeared at the coast and later offshore. The upwelling jet in Monterey Bay disappeared in August.

At 200 dbar (Fig. 8b), the upwelling jet appeared to be much reduced, both temporally, spatially and in strength. At 75 km from shore, maximum poleward flow exceeded 7 cm/s during May through July. Current meter observations at 350 m depth to the west of Point Sur, California, indicated year round poleward flow, with strongest velocities, ~15 cm/s, during the same May–July period (Collins et al., 1996).

4.2. Wind forcing

Pennington and Chavez (2000) have pointed out the importance of the relationship between upwelling favorable winds and the annual variability of hydrographic and biological properties in Monterey Bay. For this study, upwelling was calculated by using monthly estimates of geostrophically derived wind-driven offshore Ekman transports for 36°N, 122°W from April 1988 to January 2002. These data were compiled by the Pacific Environmental Fisheries Laboratory and are available at http://www.pfeg.noaa.gov/products/PFELindices.html). Ekman transports for May 1991 to December 1996 and July 1997 to June 1998 were deleted so that these data corresponded to the same time period as the hydrographic data. Calculations of the annual cycle of vertical transport from the geostrophically derived wind driven transport yielded an amplitude of 1.22 m^3/s per m of coastline, a phase that indicated that upwelling was greatest on June 8, and accounted for 74% of the variability. Integrated over half a cycle, this yields a total transport of $1.94 \times 10^7\ m^3$ per m of coastline.

Seasonal isopycnal displacements can be directly compared with the Ekman transports. The annual displacement of 25.8 (26.2) kg/m^3 isopycnal over the 100 km closest to shore was about 20% of the Ekman transport, $4 \times 10^6\ m^3$ ($5.4 \times 10^6\ m^3$) per m of coastline. The difference between the Ekman transport and the isopycnal displacements is either due to horizontal and vertical recirculation in the

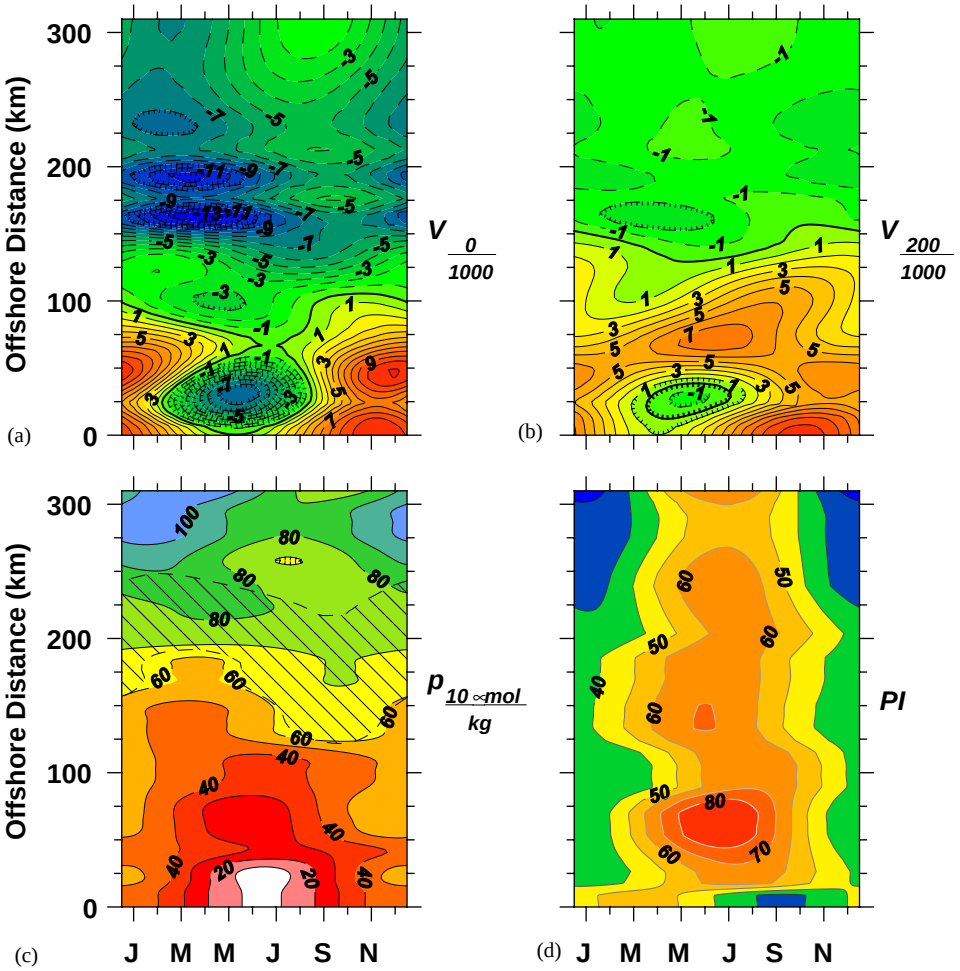

Fig. 8. Annual cycles of derived properties along Line 67. Letters beneath the abscissa correspond to months and are placed beneath tick marks that correspond to the first day of the month. (a) Geostrophic velocity at the surface relative to a 1000 dbar reference level. Contour interval is 2 cm/s. Negative isotachs (dashed lines) indicate equatorward flow. The zero isotach is highlighted. (b) Geostrophic velocity at 200 dbar relative to 1000 dbars. Contour interval is 1 cm/s. Negative isotachs (dashed lines) indicate equatorward flow. The zero isotach is highlighted. (c) Annual cycle of nutricline pressure (10 μmol/kg was used as a proxy of nutricline depth). Contour interval is 10 dbar. Hatched region corresponds to dynamic heights between 0.45 and 0.49 dynamic meters termed the CC Jet. (d) Annual cycle of productivity index. Contour interval is 10 mg C mg/(Chl-*a*).

upper ocean or to movements of isopycnals associated with accelerations of alongshore flow that were unrelated to coastal mass divergence.

4.3. Biological and chemical processes

As noted above, the CC jet was associated with a large gradient in the upper layer temperature and divided the offshore region with low nutrients, chlorophyll-*a* and primary productivity from the coastal zone where these properties were much larger. The CC jet causes a geostrophic adjustment of the nutricline that contributes to this effect. An annual nutricline cycle was constructed using 10 μmol kg^{-1} nitrate (Fig. 8c). The nutricline was about 20 dbar shallower than the 25.8 kg m^{-3} isopycnal (Fig. 7d), and its pressure ranged from 110 dbar offshore in winter to less than 10 dbar at the coast in June-July. The CC jet, overlaid on Fig. 8c, showed the geostrophic adjustment of the

nutricline from 80 to 100 dbar offshore to less than 60 dbar inshore of the jet.

The upwelling jet across the mouth of Monterey Bay was strongest in May–June, resulting in additional shoaling of the nutricline and pycnocline inshore toward the coast. Lowest temperatures and highest salinities occurred in the coastal domain during this period. The sequence of near-coastal events was that temperature was coldest in May, nitrate and offshore Ekman transport highest in early June, chlorophyll-*a* and salinity highest in late June (Fig. 7). The primary production maximum varied across this nearshore region, with largest values at 25 km from shore preceding the mid-June coastal maximum by a month (Fig 7l). The enhanced coastal high nutrient/chlorophyll-*a* region extended farthest from shore during this period.

During autumn, the CC jet slowed and moved about 80 km toward shore, poleward geostrophic flow resumed in the coastal zone, and the nutricline and pycnocline deepened. At the coast, upper-layer temperatures and salinities that were offshore in summer appeared next to the coast, which was consistent with the historical and recent descriptions of Monterey Bay hydrography (Skogsberg, 1936; Pennington and Chavez, 2000). However, note that this description was inconsistent with remotely sensed altimeter data (Strub and James, 2000). These authors described an offshore migration of the equatorward meandering jet from spring to fall, and suggested that as the jet moved offshore it became unstable, generating eddies that also propagated westward.

CC jet waters were transitional between the high-nutrient euphotic zone waters of the upwelling domain and the low-nutrient waters of the CC, and were characterized by decreasing 0–80 dbar nitrate values (Fig. 7j) and a deepening nutricline (Fig. 8c) and chlorophyll-*a* maximum (Table 1). Offshore, chlorophyll-*a* values were higher in winter than summer, as previously described (Chavez, 1995). This cycle, in combination with higher offshore primary production in spring and summer, resulted in a strong seasonal cycle offshore in primary production/chlorophyll-*a* ratios (Fig. 8d).

The waters of the California Current have biological characteristics similar to the oligotrophic waters of the North Pacific Suptropical Gyre (Winn et al., 1995). They both have deep chlorophyll-*a* maxima, and chlorophyll-*a* in the surface waters increases in the winter. This winter increase may be in part due to increased nutrient supply from deeper mixed layers, but is also the result of increases in chlorophyll-*a* per cell in response to a lower light environment associated with lower incoming solar irradiance and deeper mixed layers (Winn et al., 1995; Chavez, 1995).

5. Conclusions

The CC jet separates the eutrophic coastal region from the more oligotrophic waters of the CC. Conditions in the inshore waters are strongly seasonal and driven by (1) geostrophic adjustment of the pycnocline caused by seasonal variation of the California Current system, and (2) the cycle of upwelling favorable winds. Several important consequences follow from these dynamics. First, the high nutrient levels in the coastal domain are not a result of transport of nutrients from the north by the CC as suggested by Chelton et al. (1982). Second, the CC increases the upwelled nutrient flux through geostrophic adjustment, perhaps leading to the correlation between alongshore transport and zooplankton abundance reported by Chelton et al (1982). Third, the offshore location of the CC jet and consequently the inshore edge of the California Current is determined by the breadth and strength of the California Undercurrent and Inshore Current (when it was weak, as in mid-1998, then the California Current was closer to shore and the coastal eutrophic region was smaller). Finally, there may be considerable subduction of coastal waters and biologically active constituents beneath the CC jet. This flux is not typically accounted for in models and may be a significant fraction of biogenic export from coastal environments to the deep-sea (Barth et al., 2002). Fig. 9 illustrates the geostrophic adjustment of the CC jet inshore and the apparent downward displacement of surface-produced chlorophyll to depths below the euphotic zone along Line 67 in January 2002.

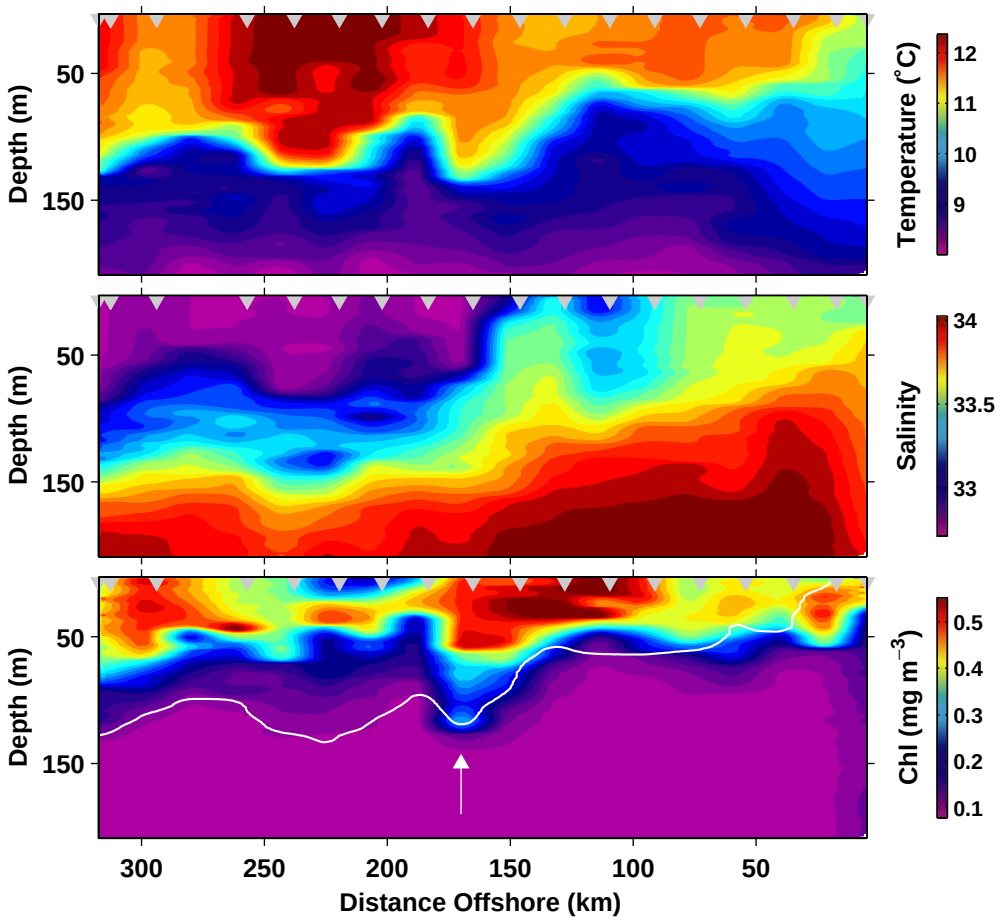

Fig. 9. Hydrobiological section along CalCOFI Line 67 in January of 2002 (upper) Temperature, °C. (middle) Salinity (lower) Chlorophyll-*a*. The 25.6 kg/m^3 isopycnal is plotted in white. The arrow marks the inshore edge of the low salinity California Current and the subduction of surface-produced chlorophyll-*a*.

Acknowledgements

This study was sponsored by the Oceanographer of the Navy, the Naval Oceanographic Office, the National Science Foundation, and the David and Lucile Packard Foundation. The *R/V Point Sur, R/V New Horizon, R/V Point Lobos, USNS DeSteiguer* and *NOAA Ship McArthur* were used for data collection activities, and the efforts of the crews of these ships are gratefully acknowledged. CGC was supported by the National Research Council. We thank John Ryan for help with preparation of figures. On the occasion of his retirement from the National Marine Fisheries Service, we thank Mr. Ron Lynn for his efforts to document and understand the California Current system that have served to guide and stimulate our studies of Central California waters. Comments from Dr. Teresa Chereskin and an anonymous reviewer improved this paper considerably.

References

Abbott, D.P., Albee, R., 1967. Summary of thermal conditions and plankton volumes measured in Monterey Bay, California 1961–1966. CalCOFI Reports 11, 155–156.

Asanuma, H., Rago, T.A., Collins, C.A., Chavez, F.P., Castro, C.G., 1999. Changes in the Hydrography of Central California Waters associated with the 1997–1998 El Niño. Technical Report NPS-OC-99-01, Naval Postgraduate School, Monterey, CA, 121pp.

Barth, J.A., Cowles, T.J., Kosro, P.M., Shearman, R.K., Huyer, A., Smith, R.L., 2002. Injection of carbon from the shelf to offshore beneath the euphotic zone in the California Current. Journal of Geophysical Research 107, 10.1029/2001JC000956.

Brink, K.H., Cowles, T.J., 1991. The Coastal Transition Zone Program. Journal of Geophysical Research 96, 14637–14647.

Chavez, F.P., 1995. A comparison of ship and satellite chlorophyll from California and Peru. Journal of Geophysical Research 100, 24855–24862.

Chavez, F.P., Pennington, J.T., Castro, C.G., Ryan, J.P., Michisaki, R.M., Schlining, B., Walz, P., Buck, K.R., McPhadyen, A., Collins, C.A., 2002. Biological and chemical consequences of the 1997–98 El Niño in central California waters. Progress in Oceanography 54, 205–232.

Chelton, D.B., 1984. Seasonal variability of alongshore geostrophic velocity off central California. Journal of Geophysical Research 89, 3473–3486.

Chelton, D.B., Bernal, P.A., McGowan, J.A., 1982. Large-scale interannual physical and biological interaction in the California Current. Journal of Marine Research 40, 1095–1125.

Collins, C.A., Castro, C.G., Asanuma, H., Rago, T.A., Han, H.-K., Durazo, R., Chavez, F.P., 2002. Changes in the hydrography of Central California waters associated with the 1997–98 El Niño. Progress in Oceanography 54, 184–204.

Collins, C.A., Garfield, N., Rago, T.A., Rischmiller, F.W., Carter, E., 2000. Mean structure of the Inshore Countercurrent and California Undercurrent off Point Sur, California. Deep-Sea Research II 47, 765–782.

Collins, C.A., Paquette, R.G., Ramp, S.R., 1996. Annual variability of Ocean Currents at 350-m depth over the Continental Slope off Point Sur, California. CalCOFI Reports 37, 251–257.

Garfield, N., Collins, C.A., Paquette, R.G., Carter, E., 1999. Lagrangian exploration of the California undercurrent. Journal of Physical Oceanography 29, 560–583.

Hickey, B.M., 1998. Coastal oceanography of Western North America from the tip of Baja California to Vancouver Island. In: Robinson, A.R., Brink, K.H. (Eds.), The Sea, Vol. 12. Wiley, New York, pp. 345–393.

Kuo, F.-Y., 1991. Monthly mean time series of temperature and salinity in Monterey Bay, 1951–1991. MS. Thesis, Naval Postgraduate School, Monterey, CA, 80pp.

Lynn, R.J., 1967. Seasonal variation of temperature and salinity at 10 meters in the California Current. CalCOFI Reports 11, 157–186.

Lynn, R.J., Simpson, J.J., 1987. The California Current System: The seasonal variability of its physical characteristics. Journal of Geophysical Research 92, 12947–12966.

Lynn, R.J., Bliss, K.A., Eber, L.E., 1982. Vertical and horizontal distributions of seasonal mean temperature, salinity, sigma-*t*, stability, dynamic height, oxygen and oxygen saturation in the California Current, 1950–1978. CalCOFI Atlas 30, State of California. Marine Research Comm., La Jolla, 513pp.

Pennington, J.T., Chavez, F.P., 2000. Seasonal fluctuations of temperature, salinity, nitrate, chlorophyll and primary production at station H3/M1 over 1989–1996 in Monterey Bay, California. Deep-Sea Research II 47, 947–974.

Rago, T.A., Locke, J.G., Collins, C.A., 1997. An Atlas of the Hydrographic Stations Off Point Sur, California, April 1988–April 1991. Naval Postgraduate School Technical Report NPS-OC-97-006, 427pp.

Rosenfeld, L.K., Schramm, R.E., Paduan, J.B., Hatcher, G.A., Anderson, T., 1994a. Hydrographic Data Collected in Monterey Bay During 1 September 1998 to 16 December 1992. Monterey Bay Aquarium Research Institute Technical Report 94-15, 549pp.

Rosenfeld, L.K., Schwing, F.B., Garfield, N., Tracy, D.E., 1994b. Bifurcated flow from an upwelling center: a cold source for Monterey Bay. Continental Shelf Research 14, 931–964.

Skogsberg, T., 1936. Hydrography of Monterey Bay, California. Thermal conditions. 1929–1933. Transactions of the American Philosophical Society 29, 1–152.

Skogsberg, T., Phelps, A., 1946. Hydrography of Monterey Bay, California. Thermal conditions, Part II, 1934–1937. Proceedings of the American Philosophical Society 90, 350–386.

Steger, J.M., 1997. Use of ship-mounted acoustic doppler current profiler data to study mesoscale oceanic circulation patterns in the Archipielago de Colon (Galapagos Islands) and the Gulf of the Farallones. Ph.D. Dissertation. Naval Postgraduate School, Monterey, CA, 154pp.

Strub, P.T., James, C., 2000. Altimeter-derived variability of surface velocities in the California Current System: 2. Seasonal circulation and eddy statistics. Deep-Sea Research II 47, 831–870.

Winn, C.D., Campbell, L., Christian, J.R., Letelier, R.M., Hebel, D.V., Dore, J.E., Fujieki, L., Karl, D.M., 1995. Seasonal variability in the phytoplankton community of the North Pacific Subtropical Gyre. Global Biogeochemical Cycles 9, 605–620.